Green Chemistry

PAPER

View Article Online
View Journal | View Issue

Open Access Article. Published on 28 April 2020. Downloaded on 10/22/2025 12:39:52 AM.
This article is licensed under a Creative Commons Attribution 3.0 Unported Licence.

Check for updates

Cite this: *Green Chem.*, 2020, **22**, 3262

Photoreforming of food waste into value-added products over visible-light-absorbing catalysts†

Taylor Uekert, Florian Dorchies, Christian M. Pichler and Erwin Reisner *

Received 8th April 2020,
Accepted 28th April 2020

DOI: 10.1039/d0gc01240h

rsc.li/greenchem

Approximately 1.3 billion tons of food waste are generated each year, resulting in societal, economic and environmental repercussions across the globe. While efforts to minimise losses and redistribute resources are underway, vast quantities of food waste must still be managed. Photoreforming offers a simple, sunlight-driven method for transforming food waste into valuable chemicals and clean H_2 fuel, but the minimal previous research on this topic relied on expensive and UV-absorbing catalysts. Here, we utilise two precious-metal-free and visible-light-driven photocatalytic systems (CdS quantum dots in alkaline solution and carbon nitride with co-catalyst Ni_2P under pH neutral conditions) to photoreform a variety of carbohydrates, fats, proteins and real-world mixed wastes into H_2 and organic products such as formate. CdS offers higher efficiencies in alkaline media than a benchmark TiO_2|RuO_2-Pt catalyst, but carbon footprint calculations suggest that photoreforming with carbon nitride|Ni_2P in pH neutral H_2O offers a more sustainable route towards real-world application.

1. Introduction

One-third of all food produced for human consumption is lost or wasted each year.[1–3] This results in food insecurity, economic losses (~$940 billion USD per year)[4] and environmental impacts; the carbon footprint of food wastage is approximately 4.4 Gt CO_2 equivalents per year, or 8% of total global greenhouse gas emissions.[1] Food waste arises at all stages of the supply chain, from agricultural production to household consumption, and although the exact loss mechanisms differ between regions, the issue remains a global challenge.[2,3]

Much food waste is avoidable and can be addressed by improved infrastructure, knowledge transfer and marketing techniques.[5] However, even if the goal outlined by the United Nations to halve food losses by 2030 is achieved,[6] billions of tons of material will still go to waste. The majority of this waste is currently sent to landfill or incinerated, resulting in greenhouse gas emissions and a loss of energy and nutrients.[7,8] One promising alternative is anaerobic digestion, in which microorganisms produce biogas (a mixture of CH_4, CO_2 and H_2) from food waste. While this process allows for energy recovery, it has high initial capital costs, cannot use mixed waste and often produces impure biogas.[7] New technologies are therefore required to reclaim the economic and material value of food waste.

Photoreforming (PR) is one such option. In PR, electrons in a semiconductor are excited to the conduction band (CB) by sunlight and reduce water to H_2, while the photogenerated holes in the valence band (VB) drive the oxidation of an organic substrate (Fig. 1). It can therefore be considered a hybrid process between photocatalytic water splitting and organic photo-redox catalysis. PR has several unique benefits, including no external energy input beyond sunlight, applicability to small off-grid systems, compatibility with mixed and wet waste, and ability to produce pure, fuel-cell-grade H_2. This technology is thus a suitable candidate for simultaneous food waste management and fuel generation.

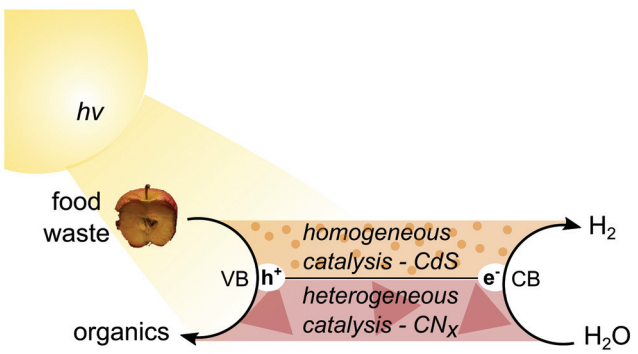

Fig. 1 Schematic diagram of food waste photoreforming over CdS/CdO_x quantum dots or $^{H2N}CN_x$|Ni_2P.

Department of Chemistry, University of Cambridge, Lensfield Road, Cambridge CB2 1EW, UK. E-mail: reisner@ch.cam.ac.uk

†Electronic supplementary information (ESI) available. See DOI: 10.1039/d0gc01240h. Raw data related to this publication are available at the University of Cambridge data repository: https://doi.org/10.17863/CAM.51830

This journal is © The Royal Society of Chemistry 2020

Open Access Article. Published on 28 April 2020. Downloaded on 10/22/2025 12:39:52 AM.
This article is licensed under a Creative Commons Attribution 3.0 Unported Licence.

While PR of simple organic molecules,[9] sugars,[10,11] biomass[12,13] and even plastic[14–16] has been reported, there has been limited research on food or mixed waste. The few publications on PR of food waste all utilised a TiO_2 photocatalyst coupled with noble metal co-catalysts such as Pt.[16,17] The efficiency and real-world applicability of these systems were therefore limited by their ultraviolet-only absorption and expense.

Here, we report visible-light-driven and noble-metal-free PR of food and mixed wastes. We select two different types of catalysts – water-soluble CdS/CdO_x quantum dots (QDs) and heterogeneous carbon nitride with a nickel phosphide co-catalyst ($^{H2N}CN_x|Ni_2P$) – to reform a range of substrates including carbohydrates, proteins and fats into H_2 and organic products under both neutral and alkaline aqueous conditions (Fig. 1). CdS/CdO_x is shown to exhibit higher activity for both H_2 evolution and formate production in alkaline conditions, but $^{H2N}CN_x|Ni_2P$ offers greater versatility over a wide pH range. Finally, we apply PR to real-world mixed wastes and provide preliminary carbon footprint calculations for the different photocatalytic systems, thereby highlighting the potential of PR to sustainably transform food and mixed waste into renewable fuel and chemicals.

2. Photocatalysis for H_2 generation

CdS/CdO_x QDs and $^{H2N}CN_x|Ni_2P$ were selected for their visible light absorption, lack of noble metals and known applicability to relevant photocatalytic processes such as H_2 evolution, pollutant degradation and organic transformations.[18,19] CdS/CdO_x QDs feature a band gap of 2.4 eV (λ < 515 nm), favourable band positions (CB −0.5 V *vs*. NHE, VB +1.9 V *vs*. NHE at pH 7),[20] and have been utilised previously to photoreform both biomass[21] and plastics[14] under alkaline conditions. Carbon nitride ($^{H2N}CN_x$) has a band gap of 2.7 eV (λ < 460 nm) and suitable band positions for PR (CB −0.85 V *vs*. NHE, VB +1.85 V *vs*. NHE at pH 7).[22,23] When coupled with an appropriate H_2 evolution co-catalyst, carbon nitride has reformed biomass (with a molecular Ni catalyst)[24] and plastics (with Ni_2P).[15] The different form factors of CdS and $^{H2N}CN_x$ also enable analysis of the impact of homogeneity *versus* heterogeneity on PR efficacy.

CdS QDs were prepared by hot-injection synthesis as described previously[25] (diameter ∼ 4.7 nm, λ_{max} ∼ 460 nm, Fig. S1†). Ligand-free QDs were used for PR as the exposed surfaces offer higher catalytic performance than ligand-capped QDs.[25] When dispersed in alkaline aqueous solution, the QDs form a thin Cd oxide/hydroxide shell (CdO_x) that prevents photocorrosion.[21,26] $^{H2N}CN_x$ was prepared from melamine at 550 °C,[27] and then loaded with a Ni_2P co-catalyst (2 wt%) as reported previously.[15] Inductively-coupled plasma optical emission spectrometry (ICP-OES) confirms that Ni_2P is present at the expected weight percentage (Table S1†). Upon addition of the co-catalyst, the visible light absorption of $^{H2N}CN_x$ is retained (Fig. S2a†) and the fluorescence emission is quenched slightly, indicating reduced radiative charge recombination (Fig S2b†). The bulk chemical properties of $^{H2N}CN_x$ are unaffected by co-catalyst addition (Fourier-transform infrared spectroscopy – Fig. S2c,† X-ray powder diffraction – Fig. S2d,† and X-ray photoelectron spectroscopy – Fig. S3†) and Ni_2P is present as agglomerates of nanoparticles on the photocatalyst surface (scanning electron microscopy and energy dispersive X-ray spectroscopy – Fig. S4†). Cyanamide-functionalised carbon nitride ($^{NCN}CN_x$), which was previously shown to enhance charge separation and photocatalytic efficiency,[24,28] was also investigated for PR with a Ni_2P co-catalyst, but offered no substantial improvement (Table S2†).

We then applied the photocatalysts to PR of food-derived substrates. All conditions, including photocatalyst[15,21] and substrate concentrations (Table S3†), were optimised for maximal H_2 evolution. Experiments with CdS/CdO_x QDs were conducted in 10 M aq. KOH, as CdS photo-corrodes at neutral or acidic pH (Table S4†).[21,26] On the other hand, $^{H2N}CN_x|Ni_2P$ functions at highly alkaline (10 M KOH), neutral (H_2O) and acidic (1 M H_2SO_4) pH, with PR in KOH outperforming H_2O by at least three times (Table S2†). It was therefore decided to study $^{H2N}CN_x|Ni_2P$ at both alkaline (for highest performance and direct comparison to CdS/CdO_x) and pH neutral (for enhanced sustainability) conditions.

In a typical optimised experiment, the substrate was pre-treated (24 h with stirring in the dark at 40 °C in KOH or 80 °C in H_2O) to initiate substrate breakdown and enhance substrate–catalyst interaction for improved PR performance.[14,15] While pre-treatment has little effect on soluble substrates such as fructose, it increases activity for recalcitrant samples like starch (Table S5 and Fig. S5†). Slightly higher pre-treatment temperatures were required in H_2O to promote solubilisation, as evidenced by a sharpening in the characteristic ^{1}H-Nuclear Magnetic Resonance (^{1}H-NMR) spectroscopy peaks of starch at 80 °C (Fig. S5†). The pre-treated mixture was combined with either CdS/CdO_x QDs or an ultrasonicated suspension of $^{H2N}CN_x|Ni_2P$ (ultrasonication has been shown to increase carbon nitride surface area and improve PR efficiency).[24] The samples were then exposed to simulated solar light (AM 1.5G, 100 mW cm^{-2}) at 25 °C under N_2 (atmospheric pressure). All H_2 measurements are background-corrected by yield without substrates (<10% of H_2 produced during PR, Table S6†), and no H_2 is detected without the photocatalyst or light (Table S7†).

A variety of carbohydrates (glucose, fructose, galactose, sucrose and starch), the amino acid glutamic acid, proteins (casein, bovine serum albumin (BSA) and beef extract) and fats (glycerol, castor oil and soybean oil) were shown to be active for PR over CdS/CdO_x in 10 M KOH and $^{H2N}CN_x|Ni_2P$ in H_2O (Fig. 2 and Table S8†). Simple soluble molecules such as sugars, glutamic acid and glycerol offer the highest H_2 yields with both catalytic systems. As the complexity of the substrate increases, activities tend to decrease. This is due to low solubilities and limited percentages of oxygenated regions that can be photoreformed. For instance, beef extract is a mixture of

Open Access Article. Published on 28 April 2020. Downloaded on 10/22/2025 12:39:52 AM.
This article is licensed under a Creative Commons Attribution 3.0 Unported Licence.

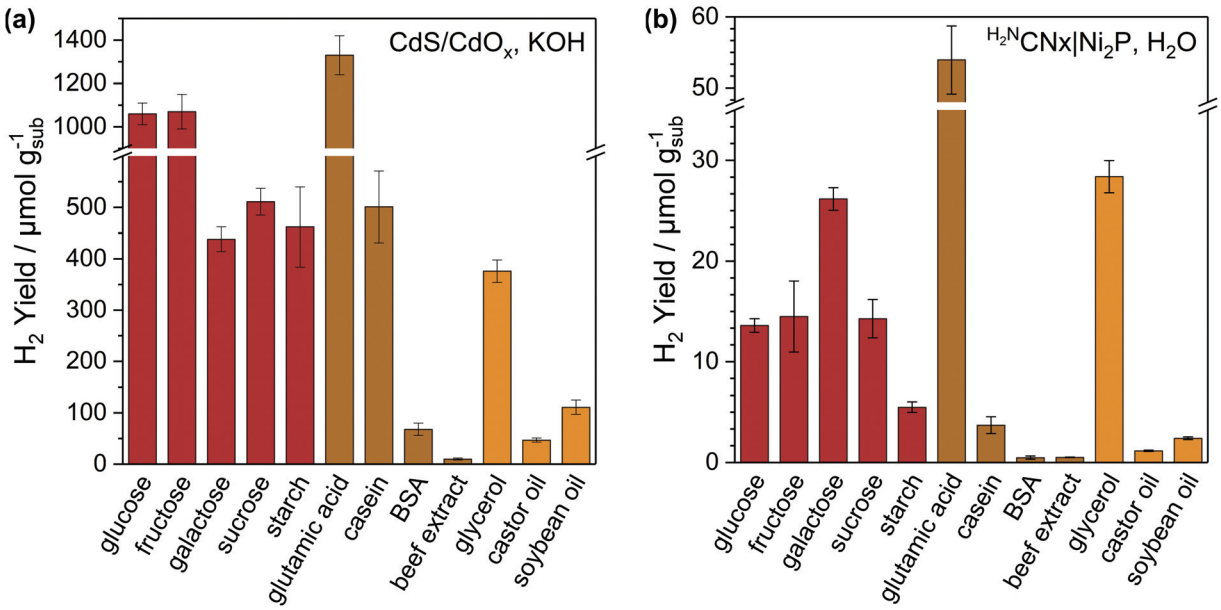

Fig. 2 Photoreforming of food-derived molecules with (a) CdS/CdO$_x$ QDs in alkaline solution and (b) ^{H2N}CN$_x$|Ni$_2$P in H$_2$O. Conditions: CdS/CdO$_x$ QDs (1 nmol) in 10 M aq. KOH (2 mL) or ^{H2N}CN$_x$|Ni$_2$P (1.5 mg mL^{-1}) in H$_2$O (2 mL); substrate (25 mg mL^{-1}) pre-treated (24 h with stirring) in 10 M KOH at 40 °C for (a) or H$_2$O at 80 °C for (b); simulated solar light (20 h, AM 1.5G, 100 mW cm^{-2}, 25 °C).

peptides, nucleotides and vitamins and offers yields of only 10.2 ± 2.0 μmol$_{H_2}$ g$_{sub}$$^{-1}$ over CdS/CdO$_x$ and 0.51 ± 0.02 μmol$_{H_2}$ g$_{sub}$$^{-1}$ over ^{H2N}CN$_x$|Ni$_2$P.

Under identical alkaline conditions, CdS/CdO$_x$ outperforms ^{H2N}CN$_x$|Ni$_2$P by 10–20 times, especially with complex substrates such as casein and starch. The homogeneous nature of CdS/CdO$_x$ QDs likely promotes access to insoluble substrates, whereas charge transfer between insoluble samples and heterogeneous ^{H2N}CN$_x$|Ni$_2$P is less favourable. CdS/CdO$_x$ QDs also benefit from wider light absorption and high charge extraction efficiency.[20] H$_2$ yields with ^{H2N}CN$_x$|Ni$_2$P are lower in H$_2$O than KOH (~10–100 and ~2–4 times less than CdS/CdO$_x$ and ^{H2N}CN$_x$|Ni$_2$P in KOH, respectively). This is due to differences in substrate solubility and breakdown, as well as the lower efficiency of Ni$_2$P in neutral *versus* alkaline solution.[29] However, ^{H2N}CN$_x$|Ni$_2$P remains active and reforms all tested substrates in H$_2$O with yields 4–15 times greater than CdS under the same conditions (Table S4†).

Casein, fructose and starch were selected for further study due to their presence in commonly discarded food items (cheese, apples and bread),[30] defined molecular formulas and range of solubilities. After 5 days of irradiation, H$_2$ conversions (measured *versus* theoretical H$_2$ yield) of 16–27% were achieved with CdS/CdO$_x$ in KOH, 3–7% with ^{H2N}CN$_x$|Ni$_2$P in KOH, and 1–4% with ^{H2N}CN$_x$|Ni$_2$P in H$_2$O (Table S9†). These values are competitive with previous reports of PR with cellulose (9.7%)[21] and polyethylene terephthalate (PET, 16.6%)[14] over CdS/CdO$_x$ in 10 M KOH, as well as PET PR (4.4%)[15] with ^{NCN}CN$_x$|Ni$_2$P in 1 M KOH. The external quantum yields with fructose – 2.73% for CdS/CdO$_x$ and 0.026% and 0.005% for ^{H2N}CN$_x$|Ni$_2$P in KOH and H$_2$O, respectively (Table S10†) – are also comparable to those reported for CdS/CdO$_x$ with cellulose (1.2%)[21] and ^{NCN}CN$_x$|Ni$_2$P with PET (0.035%).[15] All systems remained active after 5 days, suggesting that higher total conversions could be achieved at longer timescales.

Although CdS/CdO$_x$ QDs agglomerate during long-term PR (transmission electron microscopy, Fig. S6†), they appear to remain chemically robust as only 3.5% of the Cd content leaches into solution after 5 days (ICP-OES, Table S1†). The stability of ^{H2N}CN$_x$|Ni$_2$P, on the other hand, differs greatly depending on the aqueous conditions utilised. In KOH, only 4% of Ni dissolves into solution after 5 days of PR (Table S1†). The Ni content is likely stabilised in alkaline conditions by the formation of Ni(OH)$_2$ on the Ni$_2$P surface.[29,31] In contrast, 60% of Ni leaches into solution during PR in H$_2$O (Table S1 and Fig. S7†). Yet this does not appear to affect efficiency, as evidenced by the nearly constant activity of ^{H2N}CN$_x$|Ni$_2$P during long-term fructose PR (Table S11†). Improved interaction between ^{H2N}CN$_x$ and Ni$_2$P would help prevent leaching and promote catalyst recyclability. In the future, heterogeneous ^{H2N}CN$_x$|Ni$_2$P could be easily separated from the PR solution by centrifugation and re-used,[15] whereas immobilisation of the water-soluble CdS/CdO$_x$ QDs on a substrate could promote facile recycling.

For comparison, ^{H2N}CN$_x$|Pt, TiO$_2$|Ni$_2$P and TiO$_2$|RuO$_2$-Pt (which was used in the first report of carbohydrate PR)[10] were prepared and studied under identical conditions (Tables 1, S12 and S13†). CdS/CdO$_x$ remains the best-performing photocatalyst under alkaline conditions, whereas TiO$_2$|RuO$_2$-Pt offers the highest activity in H$_2$O. Of the noble-metal-free options in pH neutral solution, however, ^{H2N}CN$_x$|Ni$_2$P yields the most H$_2$. Furthermore, none of the TiO$_2$-based photocatalysts perform under visible-light-only irradiation (λ > 410 nm), whereas CdS/CdO$_x$ and ^{H2N}CN$_x$|Ni$_2$P maintain 60% and 16%

Open Access Article. Published on 28 April 2020. Downloaded on 10/22/2025 12:39:52 AM.
This article is licensed under a Creative Commons Attribution 3.0 Unported Licence.

Table 1 Comparison of photocatalysts for photoreforming of casein, fructose and starch. Conditions: pre-treated substrate (25 mg mL^{-1}); CdS/CdO$_x$ (1 nmol), ^{H2N}CN$_x$|Ni$_2$P (1.5 mg mL^{-1}), ^{H2N}CN$_x$|Pt (1.5 mg mL^{-1}, 2 wt% Pt), TiO$_2$|RuO$_2$-Pt (7.5 mg mL^{-1}, 10 wt% RuO$_2$, 5 wt% Pt), or TiO$_2$|Ni$_2$P (1.5 mg mL^{-1}); 10 M aq. KOH (2 mL) or H$_2$O (2 mL); irradiation (20 h, AM 1.5G, 100 mW cm^{-2}, 25 °C). n.m. = not measured. n.d. = not detected

			H$_2$ yield (μmol g$_{sub}$$^{-1}$)				
Light	Substrate	Aqueous condition	CdS/CdO$_x$	^{H2N}CN$_x$|Ni$_2$P	^{H2N}CN$_x$|Pt	TiO$_2$|RuO$_2$-Pt	TiO$_2$|Ni$_2$P
Full spectrum	Casein	KOH	501 ± 70	19.6 ± 3.3	65.4 ± 3.3	387 ± 19	21.8 ± 1.1
		H$_2$O	0.80 ± 0.06	3.72 ± 0.83	0.84 ± 0.04	12.4 ± 0.6	0.30 ± 0.02
	Fructose	KOH	1070 ± 80	57.3 ± 5.8	84.7 ± 4.2	380 ± 19	53.2 ± 2.7
		H$_2$O	1.00 ± 0.05	14.5 ± 3.5	271 ± 13	449 ± 22	11.2 ± 0.6
	Starch	KOH	462 ± 78	37.4 ± 1.6	23.2 ± 1.2	219 ± 11	23.8 ± 1.2
		H$_2$O	1.30 ± 0.08	5.50 ± 0.53	69.3 ± 3.5	159 ± 8	0.82 ± 0.05
λ > 410 nm	Fructose	KOH	644 ± 36	8.97 ± 0.45	n.m.	n.d.	n.d.
		H$_2$O	0.58 ± 0.03	2.34 ± 0.20	n.m.	n.d.	n.d.

of their activity, respectively (Tables 1, S7 and S12†). While further activity enhancements are necessary in the future, the application of CdS/CdO$_x$ QDs and ^{H2N}CN$_x$|Ni$_2$P to a wide range of food-derived substrates is an encouraging proof-of-concept for efficient visible-light-driven and noble-metal-free PR of food waste.

3. Substrate oxidation

Complete substrate conversion yields H$_2$ and CO$_2$, but the economic feasibility of PR would be enhanced if substrate oxidation generated value-added chemicals rather than CO$_2$. ^{1}H-NMR spectroscopy was used to identify the liquid oxidation products of casein, fructose and starch (Fig. 3 and S8†). All peak assignments were determined by comparison to authentic samples (Fig. S9†). Unidentified oxidation products are labelled (x) and unlabelled peaks are from the substrate itself. Where possible, ^{13}C-NMR spectroscopy (Fig. S10†) and high-performance liquid chromatography (HPLC, Fig. S11†) were utilised to verify the liquid oxidation products, and mass spectrometry was used to analyse any additional gaseous products (Fig. S12†).

After 4 days of PR with CdS/CdO$_x$ QDs in alkaline conditions, casein oxidises to formate and other unidentified products (Fig. 3a and Table 2); these molecules likely originate from oxidisable amino acids such as glutamic acid within the casein structure.[32] Fructose analysis is more complex because alkaline pre-treatment yields a range of substrates,[33,34] with glucose, mannose, arabinose, erythrose, lactate (ii, iii) and formate (i) identifiable by NMR spectroscopy (Fig. S5 and Table S14†) and/or HPLC (Fig. S11b, also see ESI† for mechanistic details). It is thus challenging to differentiate between hydrolysis and oxidation products. However, quantitative ^{1}H-NMR spectroscopy shows that formate concentrations increase after fructose PR with CdS/CdO$_x$ QDs, indicating that formate is also an oxidation product (Fig. 3b and Table 2). Finally, starch hydrolyses to its monomer glucose, oligomers such as maltose and maltotriose, lactate and gluconate (Fig. S11d†), with formate detected as an oxidation product (Fig. 3c and Table 2).

Formate tends to photoreform over CdS/CdO$_x$ more slowly than the initial substrates (147 μmol$_{H_2}$ g$_{sub}$$^{-1}$ after 20 h *versus* 501, 1070 or 462 μmol$_{H_2}$ g$_{sub}$$^{-1}$ with casein, fructose or starch, respectively; Table S8†), which accounts for its accumulation in solution. This behaviour can perhaps be attributed to repulsion from the negatively-charged catalyst surface (Fig. S13†).[21] The presence of large quantities of formate indicates that partial substrate conversion is a common pathway. Nevertheless, some complete conversion is also achieved, as CO$_3$$^{2-}$ is evident in ^{13}C-NMR spectroscopy (Fig. S10a†). The same array of products is observed after PR with ^{H2N}CN$_x$|Ni$_2$P in 10 M NaOD, although formate concentrations tend to be less than with CdS/CdO$_x$ due to the lower efficiency of the carbonaceous catalyst (Fig. S8, S10b† and Table 2).

Under neutral PR conditions with ^{H2N}CN$_x$|Ni$_2$P, the oxidation products CO$_2$ (Fig. S12†) and formate (Fig. 3 and Table 2) are observed from casein, fructose and starch. However, the mechanism varies in H$_2$O *versus* KOH. In contrast to the alkaline case, pre-treatment of fructose in H$_2$O does not alter the original sugar (Fig. S11a†). PR of the pure fructose in H$_2$O may proceed by ring-opening followed by C–C cleavage to shorter aldoses, a process that releases large quantities of formate (see ESI† for mechanistic details).[35] It is thus expected that the oxidation products of fructose observed by ^{1}H-NMR spectroscopy (Fig. 3e and Table 2) and HPLC analysis (Fig. S11a†) include formate (i), as well as lactate (ii, iii), acetate (iv) and gluconate.[36] 40% of the produced formate can be extracted with heptanol by a facile procedure[37] (Table S14†). Starch remains an oligomer after pre-treatment in H$_2$O, as only species with higher molecular weights than the glucose trimer maltotriose are observed by HPLC (Fig. S11c†). PR then proceeds by the same mechanism as for fructose,[35] with formate (i) and acetate (iv) again apparent as oxidation products (Fig. 3f, S11c† and Table 2).

The presence of different species after pre-treatment (pure sugar in H$_2$O *versus* a mixture of hydrolysis products in KOH) as well as different consumption rates of the oxidation intermediates (*e.g.* formate reforms much faster in H$_2$O than KOH) likely account for some of the observed variations in PR efficacy between neutral and alkaline conditions (Table S8, also see cell potentials on page S2 of the ESI†). Future work

Open Access Article. Published on 28 April 2020. Downloaded on 10/22/2025 12:39:52 AM.
This article is licensed under a Creative Commons Attribution 3.0 Unported Licence.

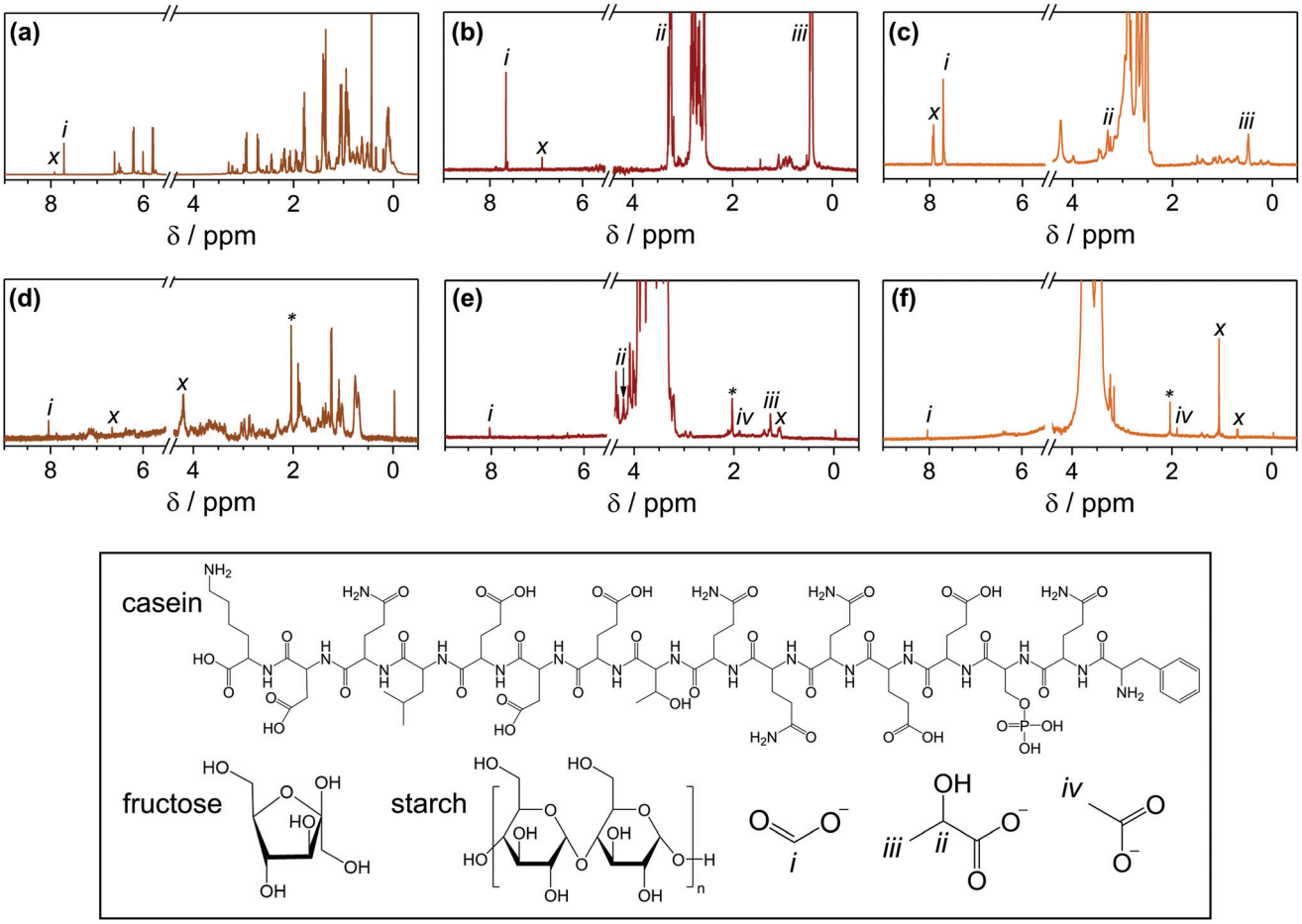

Fig. 3 ^{1}H-NMR spectroscopy of (a) casein, (b) fructose and (c) starch after photoreforming with CdS/CdO$_x$ QDs in 10 M NaOD; and (d) casein, (e) fructose and (f) starch after photoreforming with ^{H2N}CN$_x$|Ni$_2$P in D$_2$O. Chemical structures of casein, fructose, starch, formate, lactate and acetate, and their peak assignments are shown at the bottom. (*x*) are unassigned oxidation products, (*) are trace amounts of acetone contamination, and unlabelled peaks are from the substrate structure. Photoreforming conditions: CdS/CdO$_x$ QDs (0.5 nmol) in NaOD (10 M) in D$_2$O (1 mL) or ^{H2N}CN$_x$|Ni$_2$P (1.5 mg mL^{-1}) in D$_2$O (1 mL), pre-treated substrate (25 mg mL^{-1}), simulated solar light (4 days, AM 1.5G, 100 mW cm^{-2}, 25 °C).

Table 2 Quantification of formate production from photoreforming of casein, fructose and starch (25 mg) over CdS/CdO$_x$ QDs in 10 M NaOD (1 mL) and ^{H2N}CN$_x$|Ni$_2$P in 10 M NaOD and in D$_2$O (1 mL) for 4 days. Results with fructose in NaOD are corrected by the amount of formate observed after pre-treatment (see Table S14†). Maleate and potassium hydrogen phthalate were used as standards in D$_2$O and NaOD, respectively

Catalyst	Aqueous conditions	Substrate	Formate (μM)	Formate rate (μmol g_{sub}^{-1} h^{-1})
CdS/CdO$_x$	NaOD	Casein	2960	1.23
		Fructose	6280	2.62
		Starch	11 800	4.92
^{H2N}CN$_x$|Ni$_2$P	NaOD	Casein	328	0.137
		Fructose	2800	1.17
		Starch	640	0.267
^{H2N}CN$_x$|Ni$_2$P	D$_2$O	Casein	48	0.020
		Fructose	100	0.042
		Starch	56	0.023

will utilise this initial understanding of the oxidation half-reaction to alter and improve its selectivity towards value-added chemicals.

4. PR of real-world waste

Having demonstrated PR of food-derived substrates, we next studied the applicability of the photocatalytic systems to real-world food and mixed wastes (Fig. 4 and Table S15†). Pre-treated apples, bread and cheese – three of the mostly commonly discarded food items in the UK[30] – were tested for PR (Fig. 4a and Table S15†). As expected, CdS/CdO$_x$ has 8–15 times higher activity than ^{H2N}CN$_x$|Ni$_2$P in alkaline conditions, but ^{H2N}CN$_x$|Ni$_2$P also photoreforms waste in H$_2$O at moderate yields.

In all cases, fructose performs better (~3×) than apples, which is expected due to the low fructose concentration in apples (<20 wt%).[38] H$_2$ yields with starch and bread are nearly

Open Access Article. Published on 28 April 2020. Downloaded on 10/22/2025 12:39:52 AM.
This article is licensed under a Creative Commons Attribution 3.0 Unported Licence.

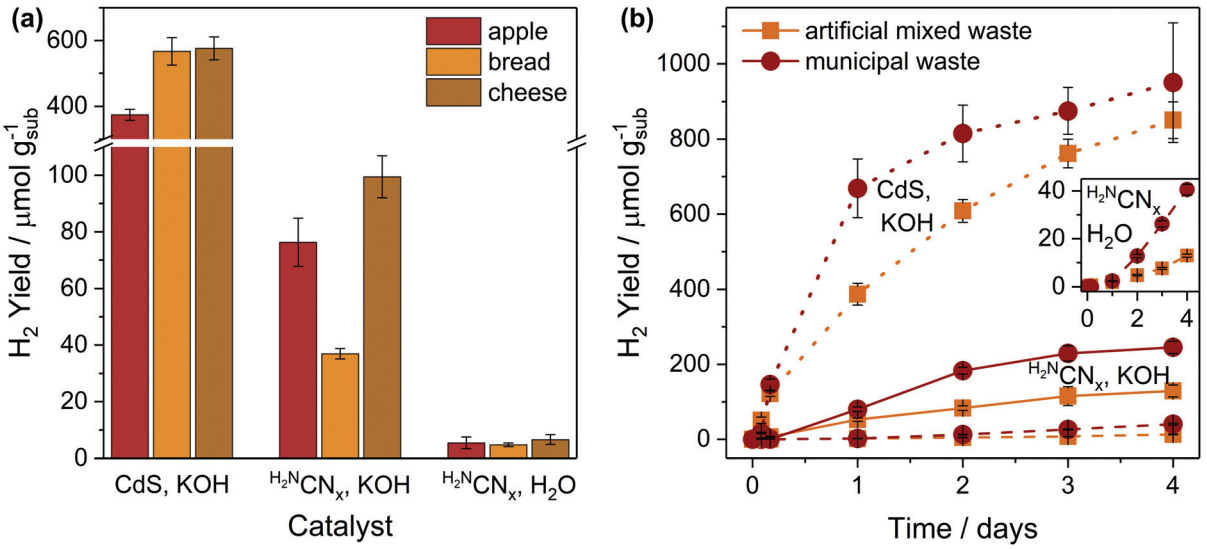

Fig. 4 Photoreforming of real-world waste, including (a) apple, bread and cheese, and (b) artificial mixed and municipal wastes; inset shows the bottom two traces ($^{H2N}CN_x|Ni_2P$ in H_2O) in more detail. Artificial mixed waste consists of 5 mg mL^{-1} each of apple, bread, cheese, cardboard and polyethylene terephthalate bottle. Conditions: CdS/CdO_x QDs (1 nmol) in 10 M aq. KOH (2 mL) or $^{H2N}CN_x|Ni_2P$ (1.5 mg mL^{-1}) in either 10 M aq. KOH (2 mL) or H_2O (2 mL); pre-treated substrate (25 mg mL^{-1} apple, bread, cheese or artificial mixed waste or 12.5 mg mL^{-1} municipal waste); simulated solar light (20 h for a, 4 days for b, AM 1.5G, 100 mW cm^{-2}, 25 °C).

identical (462 ± 78 starch and 567 ± 42 $\mu mol_{H_2}\ g_{sub}^{-1}$ bread with CdS/CdO_x in KOH; 5.50 ± 0.53 starch and 4.76 ± 0.64 $\mu mol_{H_2}\ g_{sub}^{-1}$ bread with $^{H2N}CN_x|Ni_2P$ in H_2O), as the flour in bread contains ~74–86% starch.[39] Finally, cheese performs slightly better than casein, likely because the additional carbohydrates (*e.g.* lactose)[40] in cheese reform more rapidly than casein (Table S8†). The close match between the activities of these samples and relevant pure substrates indicates that "model" molecules can predict PR performance with real-world waste.

A drawback of existing food waste management technologies is their incompatibility with mixed waste. We therefore conducted long-term PR with artificial mixed waste (equal parts apple, bread, cheese, cardboard and PET bottle) and real-world municipal waste (received from University of Leoben, Austria). Both samples were pre-treated under the conditions described previously, but any insoluble portions were removed by centrifugation to reduce light absorption and scattering by the solid residues (see Fig. S14† for ^{1}H-NMR spectra of the pre-treated samples). A lower concentration of municipal waste (12.5 mg mL^{-1}) was used since the sample was otherwise highly scattering and gelatinous. All other experimental conditions were identical to those described above.

Both artificial mixed waste and municipal waste can be photoreformed under all conditions (Fig. 4b and Table S15†). H_2 evolution initially proceeds much faster with CdS/CdO_x than with $^{H2N}CN_x|Ni_2P$ under all aqueous conditions, suggesting that the homogeneous nature of CdS/CdO_x might promote interaction with the substrates. Although the conversion rates remain low (~50–225 $\mu mol_{H_2}\ g_{sub}^{-1}\ day^{-1}$ in 10 M KOH), they already approach rates reported for bio-hydrogen production from dark fermentation of food waste (~400–4000 $\mu mol_{H_2}\ g_{sub}^{-1}\ day^{-1}$).[41] In H_2O, the overall yields of real waste PR with $^{H2N}CN_x|Ni_2P$ are up to 10 times lower than in KOH, but neutral pH offers an interesting possibility for waste separation. Plastic is not reformed in H_2O, meaning that neutral PR could potentially generate H_2 from food or cellulosic waste while simultaneously cleaning plastic. These experiments showcase the unique applicability of PR to mixed waste that is otherwise non-recyclable.

Finally, the carbon footprints (g CO_2 per kW h H_2) of PR under various conditions were estimated (see ESI† for assumptions and details). At the current *status quo*, PR with CdS/CdO_x in 10 M KOH (22% conversion after 3 days, no formate extracted, CO_3^{2-} captured in solution) has a carbon footprint of 44 600 g CO_2 per kW h H_2, with KOH accounting for 96% of that value. Unless efficient chemical recovery is implemented, the footprint of KOH is prohibitively high. PR with $^{H2N}CN_x|Ni_2P$ in H_2O (1.9% conversion after 3 days, formate extracted, no CO_2 captured) has a carbon footprint of 68 800 g CO_2 per kW h H_2, with the energy required for stirring and pre-treatment as the largest CO_2 contributors. Using renewable sources to provide energy for stirring and pre-treatment (*e.g.* solar water heating) results in a drop to −450 g CO_2 per kW h H_2. Furthermore, an ideal PR scenario in H_2O (100% conversion to H_2 and formate, renewable energy for stirring and pre-treatment) has a negative carbon footprint of −3200 g CO_2 per kW h H_2. These values compare favourably to existing H_2 evolution technologies, including steam methane reforming (23–150 g CO_2 per kW h H_2 with carbon capture), electrolysis (24–178 g CO_2 per kW h H_2 with low-carbon energy) and biomass gasification (504 g CO_2 per kW h H_2).[42] While economics will ultimately depend on catalyst safety, efficiency, selectivity and reusability, these preliminary carbon footprint calculations high-

Open Access Article. Published on 28 April 2020. Downloaded on 10/22/2025 12:39:52 AM.
This article is licensed under a Creative Commons Attribution 3.0 Unported Licence.

light the potential of PR as an environmentally-friendly method for obtaining value-added products from waste.

5. Conclusion

We have demonstrated the visible-light-driven photoreforming of food waste over two precious-metal-free photocatalytic systems. Both CdS/CdO_x QDs and $^{H2N}CN_x|Ni_2P$ reformed a variety of carbohydrates, proteins and fats into H_2, formate and CO_2 or carbonate. CdS/CdO_x offered significantly higher efficiencies, especially with insoluble substrates such as casein, whereas $^{H2N}CN_x|Ni_2P$ benefited from non-toxicity, applicability to benign (neutral pH) aqueous conditions, and a smaller carbon footprint. Mixed and municipal wastes – comprising a range of food, biomass and plastic materials – were also reformed, highlighting a key advantage of photoreforming in comparison to other food waste management technologies. With enormous quantities of food waste generated every year, photoreforming offers a unique sunlight-driven platform for transforming this resource – even when combined with other types of waste – into both valuable H_2 and organic chemicals.

6. Experimental section

Reagents

Bovine serum albumin (BSA), castor oil, D-(−)-fructose, D-(+)-glucose, maleic acid, NaOD (40 wt% in D_2O), $NiCl_2{\cdot}6H_2O$, $NaH_2PO_2{\cdot}H_2O$ and potassium thiocyanate were purchased from Fischer Scientific. Casein, D-(+)-galactose, L-(+)-glutamic acid, and starch were obtained from Acros Organics. Chloroplatinic acid (8 wt%), KOH (semiconductor grade), L-(+)-lactic acid, melamine, RuO_2 and sucrose were purchased from Sigma-Aldrich. Beef extract powder and glycerol were obtained from VWR Chemicals. D_2O (99.96 atom% D) and soybean oil were obtained from Euriso-Top and Alfa Aesar, respectively. Apples (organic royal gala apples) and bread (soft multiseed wholemeal) were purchased from Sainsbury's, cheese (mature cheddar) was purchased from Tesco Superstore, and the plastic water bottle (still Scottish mountain water) was purchased from Marks and Spencer Simply Food. Municipal waste was received from the University of Leoben, Austria.

Catalyst synthesis

Ligand-free CdS QDs were synthesised using a literature procedure reported previously.[21,25] The particle size and concentration of the CdS QDs were determined by a UV-Vis procedure based on the position and intensity of the absorption maximum.[43]

Unfunctionalised carbon nitride ($^{H2N}CN_x$) was prepared by heating melamine to 550 °C for 3 h under air according to a modified literature procedure.[27] The obtained powder was ground with a pestle and mortar. Cyanamide-functionalized carbon nitride ($^{NCN}CN_x$) was prepared according to a literature procedure.[28] $^{H2N}CN_x|Ni_2P$, $^{NCN}CN_x|Ni_2P$ and $TiO_2|Ni_2P$ were prepared as reported previously.[15]

Physical characterisation

Emission spectra (λ_{ex} = 360 nm, λ_{em} = 450 nm) were recorded on an Edinburgh Instruments FS5 spectrofluorometer equipped with a Xe lamp and integrating sphere. All samples were prepared at a concentration of 1.5 mg mL^{-1} in H_2O in a quartz glass cuvette (1 cm path length). UV-vis spectra were recorded on a Varian Cary 50 UV-vis spectrophotometer (with a diffuse reflectance accessory for CN_x samples). Fourier transform infrared spectroscopy (FTIR) spectra were collected on a Thermo Scientific Nicolet iS50 FTIR spectrometer (ATR mode). Powder X-ray diffraction (XRD) was conducted on a PANalytical Empyrean Series 2 instrument using Cu Kα irradiation. Scanning electron microscopy (SEM) and energy dispersive X-ray spectroscopy (EDX) were conducted on a TESCAN MIRA3 FEG-SEM. Samples were sputter-coated with a 10 nm layer of Cr prior to microscopy. Transmission electron microscopy (TEM) was conducted on a Thermo Scientific (FEI) Talos F200X G2 TEM. All samples were drop-cast on carbon-coated Cu grids.

Samples for X-ray photoelectron spectroscopy (XPS) were dispersed in ethanol (concentration of 5 mg mL^{-1}) and drop-cast (50 μL, 10×) onto clean FTO glass slides and dried. XPS was performed on a Thermo Fisher Scientific K-alpha$^+$ spectrometer. Samples were analysed using a microfocused monochromatic Al X-ray source (72 W) over an area of ~400 μm. Data was recorded at pass energies of 150 eV for survey scans and 40 eV for high resolution scans with 1 eV and 0.1 eV step sizes respectively. Charge neutralisation of the sample was achieved using a combination of both low energy electrons and argon ions. Two well-separated areas were selected on each sample for analysis to examine any surface heterogeneity. Data analysis was performed in CasaXPS using a Shirley type background and Scofield cross sections, with an energy dependence of −0.6.

Inductively coupled plasma optical emission spectrometry (ICP-OES) measurements were completed by the Microanalysis Service at the University of Cambridge (Department of Chemistry) on a Thermo Scientific iCAP 700 spectrometer.

Nuclear magnetic resonance (NMR) spectroscopy

^{1}H- and ^{13}C-NMR spectra were collected on either a 400 or 500 MHz Bruker Avance spectrometer equipped with a smart probe. For peak determination, samples were compared to and/or spiked with pure authentic molecules. For quantitative ^{1}H-NMR spectroscopy, samples were spiked with a known quantity of a standard solution (50 mg mL^{-1} maleic acid in D_2O for samples at neutral pH or 50 mg mL^{-1} of potassium hydrogen phthalate in D_2O for samples at alkaline pH) after photoreforming. The quantity of analyte ($m_{analyte}$) was determined with eqn (1):

$$m_{analyte} = \frac{I_{analyte}}{I_{standard}} \cdot \frac{N_{standard}}{N_{analyte}} \cdot \frac{M_{analyte}}{M_{standard}} \cdot m_{standard} \quad (1)$$

Open Access Article. Published on 28 April 2020. Downloaded on 10/22/2025 12:39:52 AM.
This article is licensed under a Creative Commons Attribution 3.0 Unported Licence.

where $I_{analyte}$ – integral of the analyte peak, $N_{analyte}$ – number of protons corresponding to the analyte peak, $M_{analyte}$ – molar mass of the analyte, $m_{standard}$ – known mass of the standard in the sample.

Substrate pre-treatment

Following a reported procedure,[14,15] substrates (typically 50 mg mL^{-1}) were soaked in aq. KOH at 40 °C or H_2O at 80 °C for 24 h with stirring at 500 rpm in air. The solution – including any undissolved pieces – was then used for catalysis as below. Real waste samples were centrifuged to remove insoluble components, as otherwise the opacity of the solution prevented light absorption by the photocatalyst.

Photocatalytic generation of H_2

For CdS samples, 1 nmol of QDs were transferred to a Pyrex glass photoreactor vial (internal volume of 7.91 mL) and the solvent was removed under vacuum with stirring. For experiments with untreated substrate, the substrate (25 mg mL^{-1}) and 2 mL of 10 M aq. KOH were added. For experiments with pre-treated substrate, 1 mL of the pre-treated mixture and 1 mL 10 M KOH were added.

For CN_x samples, a dispersion of the catalyst ($^{H2N}CN_x|Ni_2P$ or $^{NCN}CN_x|Ni_2P$) in H_2O (5 mg mL^{-1}) was ultrasonicated as described previously (10 min, pulses of 30 s at 100% amplitude followed by 5 s pauses).[24] For experiments at neutral pH, the ultrasonicated mixture (0.6 mL) was combined with H_2O (1.4 mL) and substrate (25 mg mL^{-1}) for untreated samples, or combined with the pre-treated substrate mixture (1 mL) and H_2O (0.4 mL) for pre-treated samples. For experiments at alkaline pH, the ultrasonicated mixture (0.6 mL) was combined with 15 M KOH (1.33 mL), H_2O (0.07 mL) and substrate (25 mg mL^{-1}) for untreated samples, or combined with the pre-treated substrate mixture (1 mL), 15 M KOH (0.33 mL) and H_2O (0.07 mL) for pre-treated samples. Final conditions were 2 mL of either H_2O or 10 M aq. KOH, 1.5 mg mL^{-1} catalyst, and 25 mg mL^{-1} substrate. $^{H2N}CN_x|Pt$ was prepared by ultrasonicating $^{H2N}CN_x$ according to the above procedure and then adding H_2PtCl_6 as a precursor, which forms Pt by *in situ* photodeposition. For $TiO_2|Ni_2P$ samples, the photocatalyst was added directly (no ultrasonication) to the pre-treated or untreated solution. For $TiO_2|RuO_2$-Pt samples, TiO_2 and RuO_2 were ground at a ratio of 10 : 1 with a mortar and pestle. 15 mg of the mixed catalyst were combined with 16.4 μL of H_2PtCl_6 (Pt precursor) for a final weight ratio of 100 : 10 : 5 $TiO_2 : RuO_2 : Pt$.[10]

All prepared samples were added to Pyrex glass photoreactor vials, capped with rubber septa, and purged at ambient pressure for 10 min with N_2 containing 2% CH_4 for gas chromatographic (GC) analysis. The samples were then irradiated by a solar light simulator (Newport Oriel, 100 mW cm^{-2}) equipped with an air mass 1.5 global (AM 1.5G) filter and a water filter to remove infrared radiation. Visible-light-only experiments were conducted by adding a $\lambda > 410$ nm cut-off filter. All samples were stirred at 600 rpm and kept at a constant temperature of 25 °C during irradiation. H_2 generation was monitored periodically by analysing samples of the reactor headspace gas (50 μL) by GC (see below). Overpressure within the vial is minimal.

Gas analysis

The accumulation of H_2 was measured by GC with an Agilent 7890A gas chromatograph equipped with a thermal conductivity detector and HP-5 molecular sieve column using N_2 as the carrier gas. Methane (2% CH_4 in N_2) was used as an internal standard after calibration with different mixtures of known amounts of $H_2/N_2/CH_4$. No CH_4 was detected after photocatalysis without the internal standard. CO_2 detection was carried out by mass spectrometry on a Hiden Analytical HPR-20 benchtop gas analysis system fitted with a custom-designed 8-way microflow capillary inlet to a HAL 101 RC electron impact quadrupolar mass spectrometer with a Faraday detector.

High performance liquid chromatography (HPLC)

Chromatographic separations were conducted with either a Pheomenex Rezex RCM Monosaccharide 8% Ca^{2+} column or a Phenomenex Rezex ROA-Organic Acid H^+ column. Samples were analysed in the isocratic flow mode (flow rate 0.5 mL min^{-1}) using a Shimadzu LC 20 equipped with refractive index (RID-10A) and diode array UV-Vis (λ = 190 nm) detectors. To identify particular substances in the pre-treated or photoreformed samples, retention times were compared to those of authentic samples.

Treatment of data

All analytical measurements were performed in triplicate, unless otherwise stated, and are given as the unweighted mean ± standard deviation (σ). All measurements are listed as H_2 yield per weight of substrate ($\mu mol_{H_2}\ g_{sub}^{-1}$) and activity per weight of catalyst ($\mu mol_{H_2}\ g_{cat}^{-1}\ h^{-1}$). σ was calculated using eqn (2).

$$\sigma = \sqrt{\frac{\sum (x - \bar{x})^2}{n - 1}} \tag{2}$$

where n – number of repeated measurements, x – value of a single measurement, $\bar{x}$ – unweighted mean of the measurements.

σ was increased to 5% of $\bar{x}$ in the event that the calculated σ was below this threshold.

Stoichiometric H_2 conversion calculations

Samples with 1 mg substrate in either 10 M aq. KOH or H_2O (2 mL) were prepared for photocatalysis and irradiated as described above. H_2 Conversion (%) was calculated as described in eqn (3):[15]

$$H_2\ \text{Conversion}(\%) = 100 \times \frac{n_{H_2,exp} \times n_{substrate,ideal}}{n_{H_2,ideal} \times n_{substrate,exp}} \tag{3}$$

where $n_{H_2,\ exp}$ – H_2 (mol) measured in experiment, $n_{substrate,\ exp}$ – substrate (mol) used in experiment, $n_{H_2,ideal}\ n_{substrate,ideal}^{-1}$ –

Open Access Article. Published on 28 April 2020. Downloaded on 10/22/2025 12:39:52 AM.
This article is licensed under a Creative Commons Attribution 3.0 Unported Licence.

ideal ratio of moles H_2 to substrate, as determined from the equations on page S2 of the ESI.†

External quantum yield (EQY) determination

Samples were prepared for photocatalysis as described above and added to a quartz cuvette (1 cm path length) that was then sealed with a rubber septum. The cuvette was purged with N_2 containing 2% CH_4 for 10 min and irradiated by a Xe lamp (LOT LSH302) fitted with a monochromator (LOT MSH300) focused at a single wavelength of λ = 430 nm (accurate to a full width at half-maximum of 5 nm). The light intensity was adjusted to ~1000 μW cm^{-2}, as measured with a power meter (ILT 1400, International Light Technologies). The cuvette was irradiated across an area of 0.28 cm^2. The evolved headspace gas was analysed by gas chromatography and the EQY (%) calculated with eqn (4).

$$\mathrm{EQY}(\%) = 100 \times \frac{2n_{\mathrm{H_2}} N_{\mathrm{A}} hc}{t_{\mathrm{irr}} \lambda I A} \quad (4)$$

where: n_{H_2} – amount of H_2 generated (mol), N_A – Avogadro's constant (mol^{-1}), h – Planck's constant (J s), c – speed of light (m s^{-1}), t_{irr} – rradiation time (s), λ – wavelength (m), I – light intensity (W m^{-2}), A – irradiated area (m^2).

Conflicts of interest

There are no conflicts to declare.

Acknowledgements

This work was supported by the Austrian Science Fund (Schrödinger Scholarship J-4381), the UKRI Cambridge Creative Circular Plastics Centre (CirPlas, EP/S025308/1), École Normale Supérieure Paris-Saclay and Bourse Mobilité Île-de-France (AMIS scholarship), EPSRC (NanoDTC, EP/L015978/1 and EP/S022953), and the OMV Group. XPS data collection was performed at the EPSRC National Facility for XPS (HarwellXPS), operated by Cardiff University and UCL under Contract PR 16195. We thank Dr Heather Greer for assistance with electron microscopy, Dr Annika Eisenschmidt for assistance with NMR spectroscopy, Dr Ana Belenguer for assistance with HPLC, and Ava Lage, Constantin Sahm, Dr Moritz Kuehnel and Dr Teresa Schubert for useful discussions.

References

1 Food and Agriculture Organization of the United Nations, *Food wastage footprint and climate change*, Rome, 2015.
2 J. Gustavsson, C. Cederberg, U. Sonesson, R. Van Otterdijk and A. Meybeck, Global Food Losses and Food Waste, *Food and Agriculture Organization of the United Nations*, Rome, 2011.
3 M. van den B. Verma, L. de Vreede, T. Achterbosch and M. M. Rutten, *PLoS One*, 2020, **15**, e0228369.
4 W. Britz, H. Dudu, I. Fusacchia, Y. Jafari, R. Roson, L. Salvatici and M. Sartori, *Economy-wide analysis of food waste reductions and related costs: A global CGE analysis for the EU at NUTS-II level*, Luxembourg, 2019.
5 J. Aschemann-Witzel, *Science*, 2016, **352**, 408–409.
6 K. Flanagan, K. Robertson and C. Hanson, *Reducing food loss and waste: Setting a global action agenda*, World Resources Institute, Washington, D.C., 2019.
7 S. Jain, D. Newman, R. Cepeda-Marquez and K. Zeller, *Global food waste management: An implementation guide for cities*, World Biogas Association, London, 2018.
8 A. Cerda, A. Artola, X. Font, R. Barrena, T. Gea and A. Sánchez, *Bioresour. Technol.*, 2018, **248**, 57–67.
9 Y. Pellegrin and F. Odobel, *C. R. Chim.*, 2017, **20**, 283–295.
10 T. Kawai and T. Sakata, *Nature*, 1980, **286**, 474–476.
11 D. I. Kondarides, V. M. Daskalaki, A. Patsoura and X. E. Verykios, *Catal. Lett.*, 2008, **122**, 26–32.
12 M. F. Kuehnel and E. Reisner, *Angew. Chem., Int. Ed.*, 2018, **57**, 3290–3296.
13 A. V. Puga, *Coord. Chem. Rev.*, 2016, **315**, 1–66.
14 T. Uekert, M. F. Kuehnel, D. W. Wakerley and E. Reisner, *Energy Environ. Sci.*, 2018, **11**, 2853–2857.
15 T. Uekert, H. Kasap and E. Reisner, *J. Am. Chem. Soc.*, 2019, **141**, 15201–15210.
16 T. Kawai and T. Sakata, *Chem. Lett.*, 1981, 81–84.
17 T. Sakata and T. Kawai, *J. Synth. Org. Chem., Jpn.*, 1981, **39**, 589–602.
18 Y. Wang, X. Wang and M. Antonietti, *Angew. Chem., Int. Ed.*, 2012, **51**, 68–89.
19 L. Cheng, Q. Xiang, Y. Liao and H. Zhang, *Energy Environ. Sci.*, 2018, **11**, 1362–1391.
20 Y. Xu, Y. Huang and B. Zhang, *Inorg. Chem. Front.*, 2016, **3**, 591–615.
21 D. W. Wakerley, M. F. Kuehnel, K. L. Orchard, K. H. Ly, T. E. Rosser and E. Reisner, *Nat. Energy*, 2017, **2**, 17021.
22 A. Thomas, A. Fischer, F. Goettmann, M. Antonietti, J.-O. Müller, R. Schlögl and J. M. Carlsson, *J. Mater. Chem.*, 2008, **18**, 4893–4908.
23 J. Wirth, R. Neumann, M. Antonietti and P. Saalfrank, *Phys. Chem. Chem. Phys.*, 2014, **16**, 15917–15926.
24 H. Kasap, D. S. Achilleos, A. Huang and E. Reisner, *J. Am. Chem. Soc.*, 2018, **140**, 11604–11607.
25 C. M. Chang, K. L. Orchard, B. C. M. Martindale and E. Reisner, *J. Mater. Chem. A*, 2016, **4**, 2856–2862.
26 T. Simon, N. Bouchonville, M. J. Berr, A. Vaneski, A. Adrović, D. Volbers, R. Wyrwich, M. Döblinger, A. S. Susha, A. L. Rogach, F. Jäckel, J. K. Stolarczyk and J. Feldmann, *Nat. Mater.*, 2014, **13**, 1013–1018.
27 J. Liu, Y. Liu, N. Liu, Y. Han, X. Zhang, H. Huang, Y. Lifshitz, S.-T. Lee, J. Zhong and Z. Kang, *Science*, 2015, **347**, 970–974.
28 V. W. Lau, I. Moudrakovski, T. Botari, S. Weinberger, M. B. Mesch, V. Duppel, J. Senker, V. Blum and B. V. Lotsch, *Nat. Commun.*, 2016, **7**, 12165.

 This journal is © The Royal Society of Chemistry 2020

Open Access Article. Published on 28 April 2020. Downloaded on 10/22/2025 12:39:52 AM.
This article is licensed under a Creative Commons Attribution 3.0 Unported Licence.

29 Z. Zhou, L. Wei, Y. Wang, H. E. Karahan, Z. Chen, Y. Lei, X. Chen, S. Zhai, X. Liao and Y. Chen, *J. Mater. Chem. A*, 2017, **5**, 20390–20397.
30 Waste & Resources Action Programme, *Estimates of food surplus and waste arisings in the UK*, Banbury, 2017.
31 N. Danilovic, R. Subbaraman, D. Strmcnik, K.-C. Chang, A. P. Paulikas, V. R. Stamenkovic and N. M. Markovic, *Angew. Chem., Int. Ed.*, 2012, **51**, 12495–12498.
32 B. H. Lauer, B. E. Baker and B. E. Baker, *Can. J. Zool.*, 1977, 231–236.
33 T. Vuorinen, *Carbohydr. Res.*, 1985, **141**, 319–322.
34 H. G. J. De Wilt and I. Lindhout, *Carbohydr. Res.*, 1971, **23**, 333–341.
35 K. E. Sanwald, T. F. Berto, W. Eisenreich, A. Jentys, O. Y. Gutiérrez and J. A. Lercher, *ACS Catal.*, 2017, **7**, 3236–3244.
36 Z. Zhang and G. W. Huber, *Chem. Soc. Rev.*, 2018, **47**, 1351–1390.
37 J. Reichert, B. Brunner, A. Jess, P. Wasserscheid and J. Albert, *Energy Environ. Sci.*, 2015, **8**, 2985–2990.
38 S. Musacchi and S. Serra, *Sci. Hortic.*, 2018, **234**, 409–430.
39 R. Andersson, E. Westerlund, A. C. Tilly and P. Aman, *J. Cereal Sci.*, 1992, **17**, 183–189.
40 S. Milewski, K. Zbek, Z. Antoszkiewicz, Z. Tański and A. Sobczak, *Emirates J. Food Agric.*, 2018, **30**, 107–114.
41 Y. M. Yun, M. K. Lee, S. W. Im, A. Marone, E. Trably, S. R. Shin, M. G. Kim, S. K. Cho and D. H. Kim, *Bioresour. Technol.*, 2018, **248**, 79–87.
42 The Royal Society, *Options for producing low-carbon hydrogen at scale - Policy briefing*, London, 2018.
43 W. W. Yu, L. Qu, W. Guo and X. Peng, *Chem. Mater.*, 2003, **15**, 2854–2860.